

Hyperfine splittings in $4p^55p$ configuration of ^{83}Kr using saturated absorption laser spectroscopy

J. R. Brandenberger

Department of Physics, Lawrence University, Appleton, Wisconsin 54912

(Received 8 August 1988)

Hyperfine splittings in the $2p_2$, $2p_3$, $2p_8$, and $2p_9$ states of the $4p^55p$ configuration of ^{83}Kr ($I=9/2$) have been measured using diode-laser optical pumping and saturated absorption spectroscopy. The resulting hyperfine coupling constants are in good agreement with calculated values.

I. INTRODUCTION

The hyperfine structure of the $4p^55p$ configuration of ^{83}Kr is interesting because eight of its ten states exhibit interrelated hyperfine effects. Measurements of hyperfine structures (hfs) within this configuration are numerous,¹⁻⁶ but most focus upon the same few levels and many do not attend to quadrupolar effects. In fact, reasonably precise measurements of both the magnetic and quadrupolar contributions to the ^{83}Kr hfs exist for only two states in the $4p^55p$ configuration. While this situation is understandable given the complexity of ^{83}Kr spectra, this paucity of measurements is unfortunate because modern parametric analyses of hyperfine structures require broad sets of hfs measurements drawn from single configurations.⁷ The purpose of this paper is to report a new and broader set of hfs measurements for the $2p_2$, $2p_3$, $2p_8$, and $2p_9$ states of the $4p^55p$ configuration of ^{83}Kr . No prior hfs measurements exist for three of these states.

The experimental technique employed here combines saturated absorption spectroscopy with laser optical pumping. The latter is present because the low-lying $4p^55s$ configuration of ^{83}Kr provides a multitude of final states to which the krypton atoms can relax after promotion to the $4p^55p$ states of interest. Hence we are dealing with a multilevel system in which laser excitation easily redistributes the populations. This ease with which one can depopulate any of the $4p^55s$ pseudo ground states via optical pumping is important because it significantly enhances the saturated absorption effect.^{8,9}

This work also demonstrates the utility of diode lasers in saturated absorption spectroscopy. While diode lasers have been employed extensively in molecular work, their application to high-resolution atomic spectroscopy is less common. In the present effort, GaAlAs lasers are used to optically pump and produce sub-Doppler, saturated-absorption line shapes that fully resolve the complicated hfs spectra of ^{83}Kr . Given the rapid expansion of diode-laser wavelengths into the visible, future applications and extensions of this technique are likely.

II. EXPERIMENTAL ARRANGEMENT

The target used in this work consists of a 2-cm-diam by 2-cm-long cell filled with 200 mTorr of krypton¹⁰ isotopi-

cally enriched in ^{83}Kr . To populate the $4p^55s$ pseudo ground states, a 30-MHz oscillator¹¹ excites an rf discharge in the krypton cell via external electrodes that produce rf fields of about 20 V/cm. The discharge is sufficiently weak to remain at room temperature even though the electron temperature is 5–10 eV. The number density of the krypton target is $4 \times 10^{15} \text{ cm}^{-3}$; judging from previous work,¹² we estimate the $1s_2$ through $1s_5$ populations in the $4p^55s$ configuration to be 10^{11} – 10^{12} atoms/cm³.

The experimental layout shown in Fig. 1 is conventional.¹³ Probe and pump beams counterpropagate through the target, producing saturated absorption signals of transitions connecting the $4p^55s$ and $4p^55p$ configurations. Common single-mode diode lasers¹⁴ with output powers of 5 to 40 mW and spectral widths of about 40 MHz [full width at half maximum (FWHM)] mount in a laser head equipped with two stages of thermistor sensors and Peltier heater-coolers. A controller¹⁵ for the laser provides the required current and stabilizes the temperature of the diode to ± 0.3 mK for several minutes. The controller also sweeps the laser frequency by augmenting the quiescent diode current with a current ramp derived from the sawtooth of an oscilloscope. The range of the sweep varies from 3 to 9 GHz, depending upon the hfs; its period is 50 msec. A Fabry-Pérot cavity is used to calibrate the sweep. Interferometric traces generated by this cavity and recurrent, known splittings scattered throughout our spectra confirm that the nonlinearity of the laser sweep is $< 0.1\%$ for sweeps of less than 4 GHz and $< 0.2\%$ for sweeps exceeding 4 GHz.

The scanning of the laser produces a ramp in the laser power which produces a sloping base line in the absorption spectra. To eliminate the sloping base line and suppress the Doppler-broadened components in our spectra, we employ two probe beams and matched detectors.¹⁶ The detectors are reversed-biased *p-i-n* diodes wired in opposition to the summing point of a current-to-voltage converter, so that only the difference between the two absorption signals is monitored. The probe beams, krypton cell, and detectors are carefully positioned, so that in the absence of a pump beam, the differential absorption signal is null throughout the laser sweep. Then, with the introduction of a pump beam (which crosses only one probe beam), the balance between

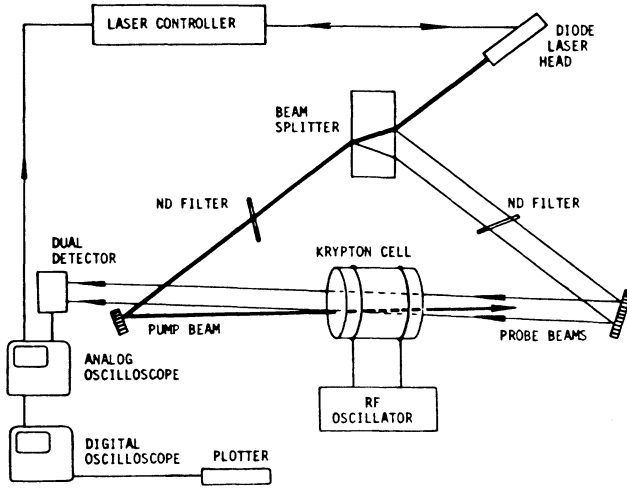


FIG. 1. Experimental layout for dual beam saturated absorption spectrometer.

the absorption signals is broken at resonance and one detects a saturated absorption signal riding on a flat base line. This dual-beam approach also suppresses common-mode signals that arise from pickup and stray light.

Neutral density filters attenuate the laser beams to optimize the tradeoff between signal size and signal width. Since the collimated beams have waists of about 1 mm, the typical probe and pump powers of 30 and 300 μW correspond to beam intensities of 10 and 100 $\mu\text{W}/\text{mm}^2$, respectively. Pump intensities are deliberately chosen to exceed the saturation intensities of the stronger lines in our spectra so as to bring out the weaker components. The laser beams are not chopped, because low laser noise obviates the need for synchronous detection.

Real-time monitoring of the differential absorption signals on the scope that sweeps the laser facilitates optimization of the experiment. These 10-mV signals exhibit signal-to-noise (S/N) ratios approaching 30. For S/N enhancement and signal capture, amplified versions of these signals pass from the first scope to a digital oscilloscope which offers a high sampling rate and 10-bit vertical resolution. By averaging 256 successive sweeps, we enhance the S/N ratio and capture the spectra in a digital format. The resulting line shapes consisting of 500 points are dumped directly to a plotter. Since both the scope and the plotter are digital, the limitations of cathode-ray optics are avoided. A typical run consisting

of four averaged spectra along with interferometric calibrations is plotted on a common chart for analysis.

III. LINE-SHAPE AND SATURATION EFFECTS

Pappas *et al.*⁸ have analyzed the present situation in which optical pumping enhances the magnitude of saturated absorption signals. These authors show that in an optically pumped, Λ -type configuration, the saturated absorption line shape for a thin target is

$$S(\nu) = A(w/2)^2[\Delta^2 + (w/2)^2]^{-1},$$

where A scales as

$$I_{\text{probe}}(I/I_{\text{sat}})(1+F)^{-1}F^{-1}(1-\Gamma_1 T)(2+\Gamma_1 T),$$

the broadening factor F is given by $F = (1 + I/I_{\text{sat}})^{1/2}$, and $w = (\gamma/2)(1+F)$ is the width of the line shape. The pump intensity I has a saturation value I_{sat} given by⁸

$$I_{\text{sat}} = (h\nu/\sigma_0\tau)[(1+\tau/T)/(2+\Gamma_1 T)],$$

in which ν is the frequency of the transition, τ is the lifetime of the upper level, Γ_1 is the spontaneous decay rate of the upper level to all lower levels except the initial one, and T is the duration of the excitation, which in our case, is dominated by the 1- μsec time interval between velocity-changing collisions for the $4p^55s$ pseudo-ground-state krypton atoms. The absorption cross section σ_0 is given by $\sigma_0 = 16\pi^2 k \mu^2 / h \gamma$, where the electric dipole moment μ for the transition satisfies $\mu^2 = 3\epsilon_0 h c^3 \Gamma_2 / 2\omega^3$. In this expression, Γ_2 is the spontaneous decay rate peculiar to the resonant pair of hfs levels. Finally,

$$\gamma = 1/\tau + 2/T + \Delta\omega_{\text{laser}}$$

is the homogeneous linewidth (FWHM); the second term in this expression reflects collisional broadening in the initial state, and the third term anticipates sizable broadening due to the spectral width $\Delta\omega$ (FWHM) of the laser.

Table I identifies the transitions, lists the $2p$ lifetimes,¹⁷ and provides estimates of the aforementioned partial decay rates Γ_1 and Γ_2 appropriate to hyperfine transitions of intermediate strength. These values of Γ_1 and Γ_2 reflect both fine¹⁷ and hyperfine branching ratios and satisfy the constraint equation $\Gamma_1 + \Gamma_2 = 1/\tau$. A dominant Γ_1 portends significant optical pumping effects, while a large Γ_2 implies little pumping but a large transition moment μ . From these parameters we calculate the saturation intensities I_{sat} and the power broadening factors F . The final column in Table I contains the experi-

TABLE I. Transitions, lifetimes, partial decay rates, and saturation parameters.

Transition	Wavelength (nm)	Lifetime ^a (nsec)	Γ_1 (10^8 sec^{-1})	Γ_2	I_{sat} ($\mu\text{W}/\text{mm}^2$)	I_{expt}	F	$(w/2\pi)_{\text{expt}}$ (MHz)
$1s_2-2p_2$	826.3	28.5	0.18	0.17	24	900	6.2	140
$1s_3-2p_3$	785.5	23.5	0.30	0.12	24	260	3.4	100
$1s_5-2p_8$	810.4	32.1	0.27	0.04	57	115	1.7	55
$1s_5-2p_9$	811.3	31.0	0.16	0.16	24	130	2.5	65

^aReference 17.

mentally observed (and broadened) widths $(w/2\pi)_{\text{expt}}$ in megahertz for hyperfine components of intermediate strength. Given these widths and F , one can infer unbroadened widths $2(w/2\pi)_{\text{expt}}/(F+1)$, all of which turn out to be about 40 MHz, thereby supporting the anticipation above that our homogeneous linewidths γ would be dominated by laser widths $\Delta\omega_{\text{laser}} = 2\pi(40 \text{ MHz})$.

IV. HYPERFINE SPECTRA

Saturated absorption spectra $S(\nu)$ that resolve the hfs splittings in the $1s_2$, $1s_5$, $2p_2$, $2p_3$, $2p_8$, and $2p_9$ states of ^{83}Kr ($I = \frac{9}{2}$) are shown in Figs. 2–5. Energy-level diagrams identify each spectral feature with a specific transition, and stick figures indicate the transition strengths assuming linear absorption and thermal populations. Although these stick figures do not apply rigorously to nonlinear absorption, they help confirm (as the figures show) the identities of the transitions in the present case where nonlinear effects are modest.

The values of the $1s_2$ and $1s_5$ splittings that appear in these figures are drawn from Jackson² and Kuiper and Friedburg.¹⁸ Since these measured splittings offer precisions that substantially exceed our capability, we use these splittings to calibrate the frequency scales of Figs. 2, 4, and 5. We note in this context that the choice of the $1s_5$ level as a pseudo ground state has four advantages: it is metastable and thus well populated in a discharge; its hfs splittings, which are known to 10 ppm, provide a convenient calibration and linearity test for the frequency

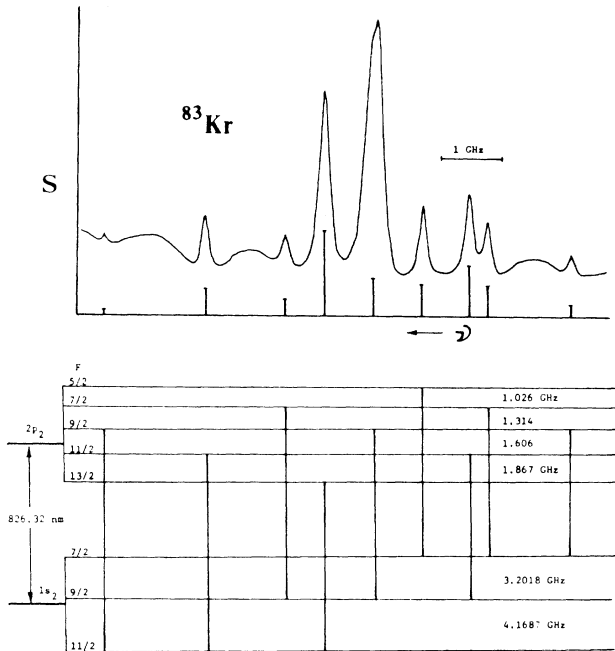


FIG. 2. Saturated absorption signal $S(\nu)$ obtained from the 826.32-nm $1s_2$ - $2p_2$ transition in ^{83}Kr . The known splittings in the $1s_2$ state are used to calibrate the frequency scale. Stick figures suggest the approximate anticipated strengths of the various hfs components. The large central feature includes contributions from other isotopes.

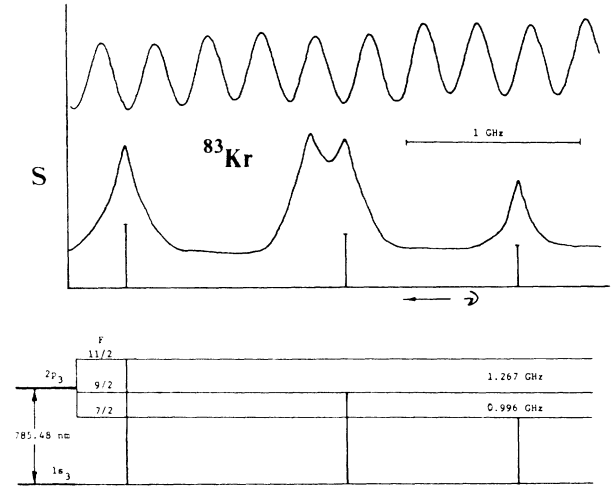


FIG. 3. Saturated absorption line shape $S(\nu)$ for the $1s_3$ - $2p_3$ transition in ^{83}Kr . The interferometric scan is used to calibrate the frequency scale.

scales of our spectra; its large hfs splittings heighten the prospect for resolution of the spectral lines that originate in it; and its multiplicity provides spectral redundancy which supports overdetermination of the hyperfine coupling constants.

Next we take up the actual determination of the $4p^55p$ hfs splittings. Consider first the $2p_3$ state shown in Fig. 3; extraction of hfs splittings from this spectrum is trivial. Using several interferometer traces and the known 308.57(5)-MHz free spectral range of our Fabry-Pérot, we calibrate the frequency scale to 0.1% and proceed to infer the $\frac{11}{2}-\frac{9}{2}$ and $\frac{9}{2}-\frac{7}{2}$ splittings to be 1.267(2) and 0.996(2)

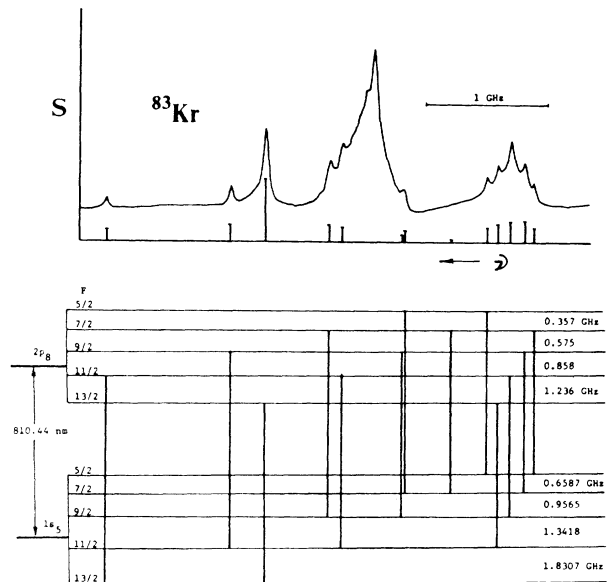


FIG. 4. Saturated absorption spectrum $S(\nu)$ for the $1s_5$ - $2p_8$ transition in ^{83}Kr . The known hfs splittings in the $1s_5$ state are used to calibrate the scan. The unidentified feature arises from even-even isotopes.

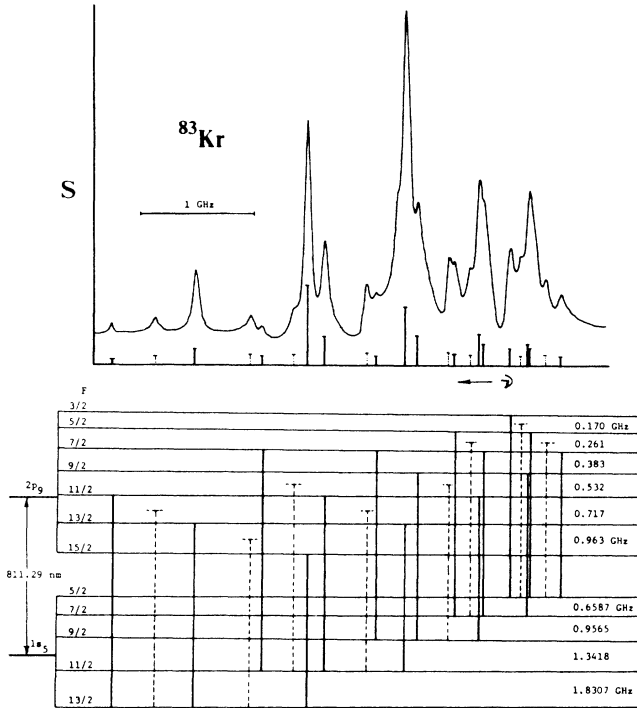


FIG. 5. Saturated absorption spectrum $S(\nu)$ consisting of 15 components in the $1s_5$ - $2p_9$ transition of ^{83}Kr at 811.29 nm. Dashed lines identify eight crossover signals.

GHz, respectively. These splittings are comparable to and harmonious with Jackson's values of 1.266(3) and 0.995(3) GHz, which are the best published values of these splittings.² We view our work on the $2p_3$ state as mainly a test of our technique. The unidentified feature in Fig. 3 arises from the residual ^{82}Kr (22%) and ^{84}Kr (5%) in our target; neither of these isotopes exhibits hfs.

The hfs spectrum shown in Fig. 2 exhibits good resolution due to the large hfs splittings in the $2p_2$ state. Even so, only one direct determination of each of the four splittings can be extracted from this spectrum because the $\frac{9}{2}$ - $\frac{9}{2}$ feature is shrouded (and rendered useless) by lines from the other isotopes. We do, however, use a few other separations to cross check the inferred splittings of 1.867(5), 1.606(5), 1.314(5), and 1.026(5) GHz. Calibration of the frequency scale for this spectrum is based upon Jackson's $1s_2$ hfs splittings;² for example, the separation between our outermost features is taken to be $3.2018 + 4.1687 = 7.3705$ GHz. Power broadening of the prominent lines in this spectrum is necessary in order to bring out the weaker features. The small humps that appear between the hfs features are attributable to imperfect nulling of the probe signals in the absence of pumping.

Figures 4 and 5 contain spectra that resolve the hyperfine structures of the $2p_8$ and $2p_9$ states; these hfs splittings have not been observed before. In both cases we use the 10-ppm $1s_5$ splittings¹⁸ to calibrate the frequency scales to better than 0.3% and simultaneously test for nonlinearity in the sweep. There is enough redundancy in the $2p_8$ spectrum to permit two independent determinations of each splitting. Final values for the $2p_8$ splittings are 1.236(5), 0.858(5), 0.575(5), and 0.357(5) GHz.

The unidentified feature in Fig. 4 stems once again from the even-even isotopes.

Our most complex spectrum involves the $2p_9$ state, as shown in Fig. 5. This spectrum includes 15 normal features and 8 crossover signals identified by the dashed lines. There is adequate resolution and redundancy in this spectrum to permit multiple determinations of all but the smallest splitting. Final values for the $2p_9$ splittings are 0.963(5), 0.717(7), 0.532(8), 0.383(9), 0.26(1), and 0.17(2) GHz. The crossover resonances were ignored in these determinations.

V. HYPERFINE COUPLING CONSTANTS AND DISCUSSION

Hyperfine coupling constants A and B which characterize the hfs splittings in a single fine-structure state are defined by the expression

$$\nu_F = \nu_J + AC/2 + B[3C(C+1)/4 - I(I+1)J(J+1)] \times [2I(2I-1)J(2J-1)]^{-1}, \quad (1)$$

where ν_J is the frequency of the unperturbed fine-structure level of known J , $I = \frac{9}{2}$ is the nuclear spin of ^{83}Kr , and $C = F(F+1) - J(J+1) - I(I+1)$. For the $2p_2$ ($J=2$), $2p_3$ ($J=1$), $2p_8$ ($J=2$), and $2p_9$ ($J=3$) states of interest here, F ranges from $\frac{3}{2}$ to $\frac{15}{2}$. By subtracting Eq. (1) from itself for adjacent pairs of hfs levels in a given $2p$ state, one can derive $2J$ linear equations that relate the set of hfs splittings $\Delta\nu = \nu_F - \nu_{F-1}$ to a single pair of coupling constants (A, B). When $J > 1$, the evaluation of (A, B) becomes overdetermined, and we solve the resulting $2J$ simultaneous linear equations graphically in order to determine the single pair (A, B) that best characterizes the set of hfs splittings. The slight scatter in the intersections of these straight lines about the best value (A, B) provides a measure of the internal consistency of the splittings and the uncertainty in A and B .

The results of reducing our hfs splittings to coupling constants (A, B) for the $2p_2$, $2p_3$, $2p_8$, and $2p_9$ states are collected in Table II along with results from three previous experimental investigations of the $2p_3$ state. Theoretical values (A, B)_{theory} determined by Husson *et al.*⁴ are shown in the final column of the table. These theoretical coupling constants were determined by parametric analysis in which experimental values of (A, B) from the $1s_2$, $1s_4$, $1s_5$, $2p_3$, $2p_4$, and $2p_7$ states of ^{83}Kr were used as input information. Notably and necessarily lacking as input to these calculations was information on the $2p_2$, $2p_8$, and $2p_9$ hyperfine structures since the splittings in these three states were unknown at the time.

The first point to notice in Table II is the excellent agreement (to nearly 0.1% in A_{expt}) between the various experimental determinations of the hfs coupling constants (A, B)_{expt} for the $2p_3$ state. One also notes the good agreement between (A, B)_{expt} and (A, B)_{theory} for the $2p_3$ state, but this fact is neither new nor surprising since Husson *et al.* used the experimental $2p_3$ coupling constants (among others) to determine their values of (A, B)_{theory}, as mentioned above. The most important

TABLE II. Hyperfine coupling constants A and B in gigahertz for $4p^55p$ configuration of ^{83}Kr .

State	This work		Jackson ^a		Husson <i>et al.</i> ^b		Gerhardt <i>et al.</i> ^c		Theory ^b	
	A	B	A	B	A	B	A	B	A	B
$2p_2$	-0.291(1)	+0.03(2)							-0.2886	+0.057
$2p_3$	+0.2268(4)	+0.022(2)	+0.2266(6)	+0.021(3)	+0.2268(2)		+0.2260(3)	+0.025(2)	+0.2284	+0.021
$2p_8$	-0.156(1)	-0.41(2)							-0.1579	-0.408
$2p_9$	-0.103(1)	-0.43(3)							-0.1031	-0.432

^aReference 2.^bReference 4.^cReference 5.

point in the table is the impressive agreement between the new, heretofore unavailable values of $(A, B)_{\text{expt}}$ for the $2p_2$, $2p_8$, and $2p_9$ states and the previously calculated results $(A, B)_{\text{theory}}$ of Husson *et al.* The excellent agreement between these experimental and theoretical coupling constants testifies to the reliability of parametric analysis of hyperfine structures.

ACKNOWLEDGMENTS

This work was supported by Research Corporation; the National Science Foundation, under Grant No. CSI-8750076; and Lawrence University. It is a pleasure to acknowledge the valuable assistance of LeRoy Frahm and Harold Everson in the development of instrumentation for this work.

¹E. Rasmussen and V. Middleboe, K. Dan. Vidensk. Selsk. Mat. Fys. Medd. **30**, 3 (1955); see also earlier references cited therein.

²D. A. Jackson, J. Opt. Soc. Am. **67**, 1738 (1977).

³R. J. Champeau and J. C. Keller, J. Phys. B **11**, 391 (1978).

⁴X. Husson, J. P. Grandin, and H. Kucal, J. Phys. B **12**, 3883 (1979).

⁵H. Gerhardt *et al.*, Hyperfine Interactions **9**, 175 (1981).

⁶H. Abu Safia and X. Husson, J. Phys. (Paris) **45**, 863 (1984).

⁷K. Heilig and A. Steudel, *Physics of Atoms and Molecules A*, edited by W. Hanle and H. Kleinpoppen (Plenum, New York, 1978), p. 263.

⁸P. G. Pappas *et al.*, Phys. Rev. A **21**, 1955 (1980).

⁹S. Nakayama, Jpn. J. Appl. Phys. **23**, 879 (1984).

¹⁰The isotopically enriched krypton was supplied by Isotec, Inc. The assay of our particular sample was ^{82}Kr (22%), ^{83}Kr (73%), and ^{84}Kr (5%).

¹¹Oscillator is a variant of the design of W. E. Bell *et al.*, Rev. Sci. Instrum. **32**, 688 (1961).

¹²J. R. Brandenberger, Phys. Rev. A **36**, 76 (1987).

¹³V. S. Letokhov and V. P. Chebotayev, *Nonlinear Laser Spectroscopy* (Springer-Verlag, Berlin, 1977), p. 119.

¹⁴Sharp laser types LT010MD, LT015MD, and LT026MD are used to drive the 810.4- and 811.3-, the 826.3-, and the 785.5-nm transitions, respectively.

¹⁵The controller is based upon a design by S. K. Lamoreaux and others of the Department of Physics, University of Washington, Seattle, WA.

¹⁶We are indebted to H. J. Metcalf for the suggestion of using dual probe beams.

¹⁷M. V. Fonseca and J. Campos, Phys. Rev. A **17**, 1080 (1978); R. S. F. Chang *et al.*, J. Chem. Phys. **73**, 778 (1980).

¹⁸H. Kuiper and H. Friedburg, Naturwiss. **48**, 69 (1961).